BIOCHEMISTRY
including biophysical chemistry & molecular biology

Article

pubs.acs.org/biochemistry

Monitoring the Kinetics of the pH-Driven Transition of the Anthrax Toxin Prepore to the Pore by Biolayer Interferometry and Surface Plasmon Resonance

Subhashchandra Naik,[†] Susan Brock,[†] Narahari Akkaladevi,[†] Jon Tally,[†] Wesley Mcginn-Straub,[§] Na Zhang,[∥] Phillip Gao,[∥] E. P. Gogol,[⊥] B. L. Pentelute,[‡] R. John Collier,[‡] and Mark T. Fisher*[,†]

[†]Department of Biochemistry and Molecular Biology, University of Kansas Medical Center, Kansas City, Kansas 66160, United States
[‡]Department of Microbiology and Immunobiology, Harvard Medical School, Boston, Massachusetts 02115, United States
[§]*forté*Bio (a division of Pall Life Sciences), Menlo Park, California 94025, United States
[∥]Protein Production Facility, University of Kansas, Lawrence, Kansas 66045, United States
[⊥]School of Biological Sciences, University of Missouri, Kansas City, Missouri 64110, United States

Supporting Information

ABSTRACT: Domain 2 of the anthrax protective antigen (PA) prepore heptamer unfolds and refolds during endosome acidification to generate an extended 100 Å β barrel pore that inserts into the endosomal membrane. The PA pore facilitates the pH-dependent unfolding and translocation of bound toxin enzymic components, lethal factor (LF) and/or edema factor, from the endosome to the cytoplasm. We constructed immobilized complexes of the prepore with the PA-binding domain of LF (LF_N) to monitor the real-time prepore to pore kinetic transition using surface plasmon resonance and biolayer interferometry (BLI). The kinetics of this transition increased as the solution pH was decreased from 7.5 to 5.0, mirroring acidification of the endosome. Once it had undergone the transition, the LF_N−PA pore complex was removed from the BLI biosensor tip and deposited onto electron microscopy grids, where PA pore formation was confirmed by negative stain electron microscopy. When the soluble receptor domain (ANTRX2/CMG2) binds the immobilized PA prepore, the transition to the pore state was observed only after the pH was lowered to early (pH 5.5) or late (pH 5.0) endosomal pH conditions. Once the pore formed, the soluble receptor readily dissociated from the PA pore. Separate binding experiments with immobilized PA pores and the soluble receptor indicate that the receptor has a weakened propensity to bind to the transitioned pore. This immobilized anthrax toxin platform can be used to identify or validate potential antimicrobial lead compounds capable of regulating and/or inhibiting anthrax toxin complex formation or pore transitions.

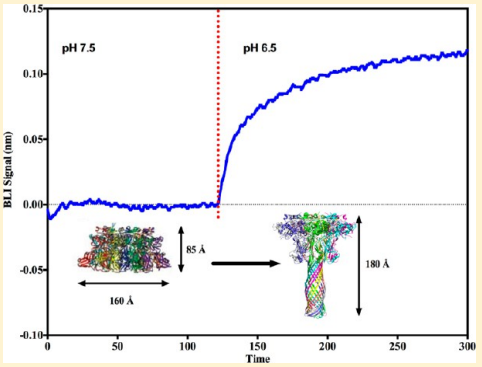

The anthrax toxin (Atx) is comprised of three different protein components: the protective antigen (PA), lethal factor (LF), and edema factor (EF). During infection, PA binds cell surface receptors (ANTXR1/TEM8 or ANTXR2/CMG2) in the plasma membrane of a host cell. A furin family protease cleaves a 20 kDa N-terminal portion of PA, allowing the PA to oligomerize into a heptameric prepore structure. This heptameric prepore can bind up to three molecules of LF and/or EF. Alternatively, PA monomers can be cleaved in solution wherein LF or EF binding facilitates PA dimerization, leading to the formation of a PA octamer, which then binds to the cell surface receptors.[1] The entire receptor-bound PA prepore LF−EF complex is endocytosed and transported to an endosomal compartment. Acidification of the endosomal compartment (pH 5.5−5.0) leads to a dramatic pH-dependent conformational change of PA where the soluble ringlike prepore (~85 Å long, 144 Å wide) refolds to form a membrane-insertable PA pore with an extended β barrel tubular stem (~100 Å long) and ringlike cap. The toxic effector enzymes LF and EF are then directionally translocated from the endosome to the cytoplasm through the PA pore across the pH gradient.[2]

To improve our understanding of the kinetic transitions that occur for the anthrax toxin complex during acidification, we surmised that it may be possible to monitor the protective antigen prepore to pore conformational transition using label-free methods. Large scale protein conformational changes can be observed using surface plasmon resonance (SPR). For example, SPR was previously utilized to observe the conformational changes or unfolding that results from urea-induced unfolding of immobilized luciferase, lysozyme, and RNase proteins.[3,4] The SPR signal is dependent on the refractive index and changes in the dielectric medium in the immediate vicinity of the protein bound to the sensor surface. Significant protein unfolding

Received: June 4, 2013
Revised: August 19, 2013
Published: August 21, 2013

dx.doi.org/10.1021/bi400705n | *Biochemistry* 2013, 52, 6335−6347

exposes buried hydrophobic residues, leading to changes in the local water structure and hence the refractive index. The only caveat for monitoring conformational changes during unfolding occurs in instances where proteins interact with the negatively charged CMD (carboxymethyldextran) matrix due to electrostatic interactions during pH-induced unfolding (pH 4−10).[5] When matrix effects are specifically avoided, conformational changes due to unfolding are readily observable.[3,4] Naturally, protein denaturation changes often generate signals that are much weaker than signals observed for protein−protein interactions. On the basis of the structural properties of the PA pore barrel, it was surmised that the transitioned PA pore will not interact with the negatively charged CMD SPR matrix because of intrinsic electrostatic repulsion. Specifically, the pore tip is negatively charged at the end of the barrel because of the concentration of negatively charged glutamic and aspartic acid residues (within the pore tip interior lumen).

We also examined the feasibility of using biolayer interferometry (BLI) as a detection platform to monitor the conformational change accompanying the prepore to pore unfolding−refolding transitions. Unlike SPR matrices, the BLI biolayer should allow us to position the PA prepore away from the biosensor surface, thus avoiding interfering matrix effects. BLI primarily detects changes in protein thickness because changes in the reflectance interference wave pattern between the sample and an internal reflectance reference layer result in a phase shift (Δ in nanometers), and these real-time changes can be followed in both kinetic and quantitative modes. In all instances tested to date, protein−protein or protein−ligand interactions that can be observed in SPR are also observed using BLI measurements. Moreover, because BLI is a rapid dip and read procedure, it is a particularly attractive technique for high-throughput development.

As the PA prepore undergoes a major unfolding−refolding transition during acidification, it forms a long β barrel pore structure that can insert into lipid membranes. This prepore to pore conformational transition results in a change in length from ∼85 to ∼170−180 Å. If this PA prepore complex is positioned correctly above the biosensor surface, this large change should be capable of being observed by SPR and BLI methods. In both instances, any changes in the pore length should result in positive deflections in both label-free signals. Once the pore is formed, it no longer undergoes the transition back to the prepore state,[6,7] leading to the additional prediction that any observed upward deflection in signal should remain and not return to the original baseline position of the prepore state in neutral pH solutions.

The optimal orientation of the PA prepore on a biosensor surface should position the prepore so that the β barrel will form roughly perpendicular to the biosensor surface. To accomplish this, the PA prepore was bound to an orientation specific thiol-attached truncated version of the lethal factor (LF_N) (N-terminal prepore binding domain). For the SPR and BLI experiments, this particular orientation ensures that (1) the large scale unfolding−refolding β barrel formation would point away from the biosensor surface and (2) the PA pore will be positioned ∼20 Å above the biosensor matrices, thereby weakening any pH-dependent matrix effects on the protein unfolding−refolding events. This particular platform construction was previously used for assembly and formation of LF_N−PA pore−nanodisc complexes for EM analysis.[8,9] In that previous structural work, the orientation of the disulfide-immobilized LF_N construct [containing a cysteine replacing a glutamate at position 126 (E126C) within an exterior β turn] on a bead surface provided optimal prepore binding for the transition from the prepore to PA pores. Once the PA pore had formed, a lipid nanodisc could be assembled around the newly exposed PA pore hydrophobic membrane insertion region. The PA pore nanodisc complexes eluted from this bead support result in a rapid purification procedure that allows one to easily visualize these complexes using electron microscopy.[8] This orientation specific binding of the PA prepore to the LF_N-positioned platform is based on the determined LF_N−PA prepore crystal structures by Krantz and co-workers.[10]

Using these label-free orientation specific PA−LF_N platforms, one can directly measure the kinetics of the prepore to pore transition conformational change as the pH is changed from 7.5 to a final pH value ranging from 6.75 to 5.0. In addition, one can determine if this pH-dependent pore transition is slowed or inhibited when a soluble receptor domain (ANTRX2) initially binds to the prepore state. The orientation of the hydrophobic PA pore tip away from the biosensor surface should also allow one to examine the binding of the lipid micelle to this hydrophobic region. The micelles that will be used are somewhat uniform in size and are comprised of a matrix scaffold protein (MSP)/cholate/POPC mixture.[11] Finally, if the LF_N-bound PA prepore or pore complex is successfully attached to BLI biosensors through reversible sulfhydryl linkages, it should be possible to remove these complexes and deposit these complexes onto EM grids to validate the PA pore transition using electron microscopy.[8]

EXPERIMENTAL PROCEDURES

Materials and Instrumentation. The SPR measurements were taken on a commercially available CM5 (carboxymethylated dextran matrix) chip (GE healthcare) using a Biacore 3000 instrument (GE healthcare). CM5 is a general-purpose chip that allows one to perform detailed quantitative interaction studies for analyzing the interaction kinetics, affinity, concentration, and binding between various biomolecules such as small organic molecules, proteins, lipids, carbohydrates, and nucleic acids. The BLI measurements were taken on an Octet 96 Red instrument at the *forte*Bio facility in Menlo Park, CA, and with the new single-channel BLItz instrument (*forte*Bio) installed in this laboratory. PA, LF_N (E126C Cys mutant of the N-terminally truncated lethal factor), and CMG2 were purified as outlined previously.[8,12] PDEA was purchased from GE healthcare. Sulfo-NHS, EDC, and L-cysteine hydrochloride were purchased from Sigma. Sodium chloride, sodium acetate, and sodium borate used in making the buffers were also purchased from Sigma.

Immobilization of PA. The immobilization of PA onto both the SPR and BLI biosensors was achieved via noncovalent affinity binding to an optimally oriented LF_N E126C construct that can be covalently linked through a sulfhydryl linkage to the biosensors. Specifically, for both SPR and BLI, a thiol surface utilizing EDC, NHS, and 2-(2-pyridinyldithio)ethaneamine hydrochloride (PDEA) (Figure 1) was initially generated. EDC and NHS were mixed in a 1:1 molar ratio and allowed to incubate with the biosensor surface for 7 min to activate the surface. PDEA dissolved in 0.1 M borate buffer (pH 8.3) was then allowed to covalently couple to the activated surface for 5 min to generate the activated thiol surface. The thiol surface was then incubated with 100 nM LF_N in 10 mM acetate buffer (pH 5.0) to generate a disulfide linkage through the lone cysteine on LF_N E126C. Excess reactive thiol groups remaining on the surface were then quenched using a solution of 50 mM cysteine in 1 M sodium chloride, 10 mM sodium acetate buffer (pH 5.0). The resulting

dx.doi.org/10.1021/bi400705n | *Biochemistry* 2013, 52, 6335−6347

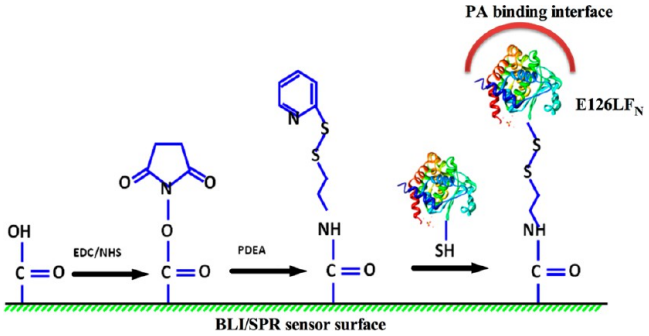

Figure 1. Chemical coupling to orient the PA prepore on Biosensor surfaces. EDC- and NHS-activated BLI or SPR biosensor surfaces were covalently modified with PDEA to produce a thiol-reactive coupling surface. LF_N E126C (PDB entry 1J7N)[33] was covalently immobilized onto the sensor via a disulfide linkage to position the LF_N–PA prepore binding interface to point away from the biosensor surface. This orientation ensures that the PA prepore will bind to the thiol-linked immobilized LF_N in a manner where the PA pore β barrel will form in direction pointing away from the biosensor surface (see PDB entry 3KWV).[10]

biosensor surfaces now contained immobilized LF_N properly oriented to bind to the PA prepore. Various concentrations of PA were then incubated with the immobilized LF_N for 10 min to bind and immobilize PA. The PA prepore binds to LF_N with a high binding affinity (K_d = 1 nM),[13] and the off rate is negligible within the time of the experiment, indicating that PA remains tightly bound to the sensor surface during the course of the pH jump experiments. Once they had undergone the transition, the PA pore-attached biosensors were also used as reference surfaces to measure solvent bulk effects that were subsequently used for baseline correction purposes for both BLI and SPR.

Measuring the Formation and Kinetics of the Pore Translocon Using SPR and BLI. *SPR.* All label-free experiments were conducted at 25 °C. Once the PA is immobilized, an acidic buffer under a variety of pH conditions (6.75–5.0) was allowed to flow over the biosensor surface at a rate of 5 μL/min and the response recorded. The experimental kinetic time course was recorded at pH ≤6.75 for 5 min followed by a chase with a neutral-pH buffer [50 mM Tris, 50 mM KCl, 10 mM $MgCl_2$, and 0.5 mM EDTA (pH 7.5)]. Any bulk effects (signal change caused by a change in buffer composition and pH) that are observed were subtracted from the initial sensorgram by repeating the experiment utilizing the same biosensor where PA had already undergone the irreversible transition. In this way, the bulk effects of solvent (e.g., small changes in the refractive index) could be subtracted from the original uncorrected sensorgram signals. Each prepore–pore transition experiment was minimally repeated twice at each pH with the SPR platform.

BLI. All kinetic experiments were conducted at 25 °C. The formation of the pore translocon was initiated by acidification of the immobilized PA using most of the protocols noted above. The BLI pore transition measurements were taken by dipping the PA-immobilized biosensor in an acidic buffer [30 mM MES, 30 mM CHES, and 30 mM phosphate (pH 5.0–7.0)] in which the platform holding the test solution was agitated rapidly (2000 rpm). The minimal number of experiments for each pH value using the BLI platforms was three. Via a comparison of SPR and BLI experimental platforms used for this work, more individual runs per day could be simultaneously performed with the multiple-channel BLI instrumentation (Octet Red 96). An entire set of pH series were also be run within a short time period using the single-channel BLI unit (BLItz).

The BLI data were analyzed using GraphPad Prism to obtain fits of the data to the kinetics of the PA transition. The kinetic traces were determined to have a minimum of three different phases [an initial burst fast phase (k_1), an intermediate medium phase (k_2), and the final slow phase (k_3) before saturation]. The data were analyzed by nonlinear fitting using a three-exponential function.

$$y = y_\infty + a(1 - e^{-k_1 t}) + b(1 - e^{-k_2 t}) + c(1 - e^{-k_3 t})$$

where y_∞ is the maximal signal possible and a, b, and c represent the fraction of signals for fast, medium, and slow phases of PA transitions, respectively. Similarly, k_1, k_2, and k_3 represent the rate constants for the fast, medium, and slow phases, respectively. These are compiled in Table 1, and the representative fits to the kinetic data are presented in Figure 2 of the Supporting Information. The goodness of fit was analyzed by examining the residual plots.

Table 1. Kinetic Data of PA pH-Induced Transitions

	SPR	BLI		
PA transition pH	$t_{1/2}$[a] (s)	k_1 (s^{-1})	k_2 (s^{-1})	k_3 (s^{-1})
6.75	1.5	0.190 ± 0.005	0.029 ± 0.001	0.005 ± 0.0009
6.5	1.5	0.813 ± 0.016	0.09 ± 0.005	0.006 ± 0.0004
6.0	<1	0.872 ± 0.021	0.082 ± 0.004	0.010 ± 0.0005
5.5	<1	1.143 ± 0.024	0.076 ± 0.024	0.008 ± 0.0004
5.0	<1	1.095 ± 0.018	0.025 ± 0.004	0.010 ± 0.0041

[a]Time to reach half of the complete reaction amplitude due to inadequate data collection at early time points via SPR vs BLI (SPR data points were collected every 0.5 s, whereas BLI data points were collected every 0.2 s).

Measuring the PA Pore Transition in the Presence of Soluble Receptor CMG2. The PA was immobilized by the method described above. For SPR, soluble receptor CMG2 (500 nM) was then injected at a flow rate of 5 μL/min and allowed to bind to the LF_N-immobilized PA prepore to obtain a saturated binding response. For BLI, the LF_N-immobilized PA prepore biosensor was dipped into an agitated solution containing the CMG2 receptor at the same concentration. With SPR, once the LF_N–PA prepore–CMG2 complex was formed, the effects of the complex on the PA pore transition were recorded as the acidic buffer flowed over the chip-immobilized LF_N–PA prepore–CMG2 complex for 8 min. During BLI, the initiation of the pore transition was conducted by dipping the immobilized LF_N–PA prepore–CMG2 complex biosensor into a vigorously stirred acidic buffer (platform set at 2000 rpm). After the acidic pulse, both SPR and BLI biosensor surfaces were restored to neutral-pH conditions with either a Tris-based buffer [50 mM Tris, 50 mM KCl, 10 mM $MgCl_2$, and 0.5 mM EDTA (pH 7.5)] or a MES/CHES/phosphate-based buffer [30 mM MES, 30 mM CHES, and 30 mM phosphate buffer (pH 7.5)]. Buffer flow rates of 5 μL/min for either the acidic or the refolding buffer were employed for the SPR studies. Any observed bulk effects (change in signal caused by a change in buffer composition and pH) were subtracted using reference sensorgrams. These reference sensorgrams were generated by repeating the experiment utilizing the same biosensors that contained completely pH-induced transitioned PA pores.

dx.doi.org/10.1021/bi400705n | *Biochemistry* 2013, 52, 6335–6347

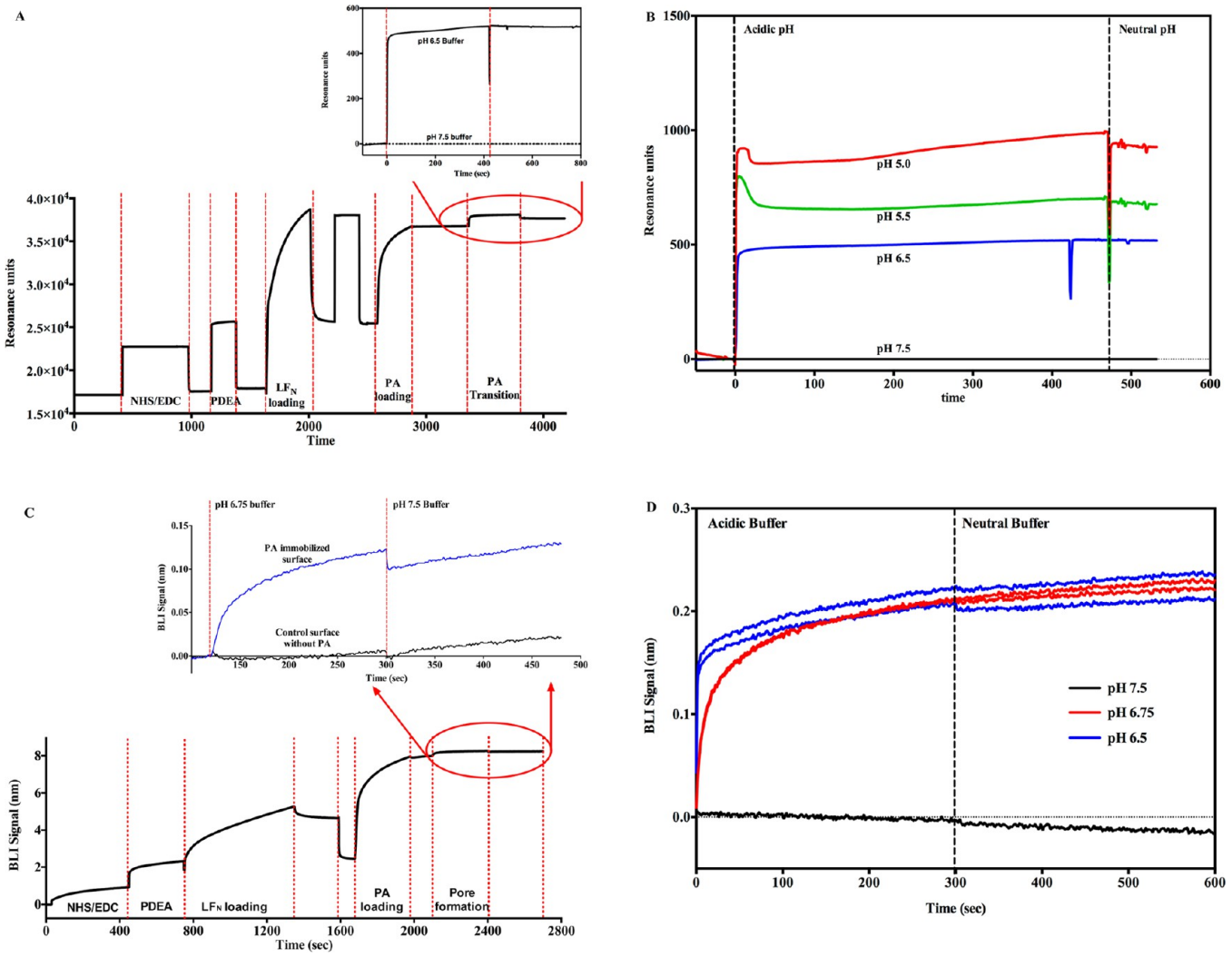

Figure 2. Monitoring the PA prepore acid-induced transition in real time by a SPR Biacore 3000 instrument (A and B) and BLI Octet system (C and D). Complete sensorgrams for SPR (A) and BLI (C) as observed for pH jumps. Magnified regions in panels A and C show the comparative amplitudes of the pH-induced changes for each label-free platform. The PA was immobilized on the biosensors and initially treated with buffers of varying acidic pH followed by the pH being increased back to neutral. The pH-induced signal changes remain once the buffer is returned to neutral pH, indicating that the origin of the signal change was irreversible. As the pH jumps approach late endosomal pH conditions (pH 5.5−5.0), the kinetic transitions become more rapid for both SPR (B) and BLI (D) [rates listed in Table 1, kinetic fits to both Octet BLI and single-channel BLI (BLItz) data in Figure 2 of the Supporting Information]. Uncorrected single-channel BLI data are shown in Figure 1 of the Supporting Information.

Electron Microscopy. BLI tips containing PDEA-immobilized LF_N−PA prepore (incubated at pH 8.0 in 30 mM MES, 30 mM CHES, 30 mM phosphate buffer) and LF_N−PA pore complexes (incubated at pH 5.0) were used as samples for electron microscopy. The immobilized complexes (prepore or transitioned pore) were removed from the BLI biosensor tips by immersing the tip directly into a 2 μL microvolume of Tris-HCl buffer containing 50 mM DTT (pH 8.0) deposited on a clean parafilm surface. After being released from the tip, the pore or prepore oligomers in the 2 μL solution were wicked onto carbon-coated Cu 300 mesh EM grids (Electron Microscopy Science) that were glow-discharged just before being used.

The untransitioned PA prepore or pH-transitioned pore complexes that eluted from the BLI tip into the 2 μL solution were allowed to incubate for 1 min on the grids and then the grids briefly dipped in three water droplets. The grids were subsequently negatively stained using 1% methylamine tungstate (pH 7). Samples were imaged with a JEOL-1200 EXII transmission electron microscope at 100 kV and the images recorded on film (Kodak SO163) by using a minimal-dose procedure at a defocus values of 0.6−0.7 μm. The micrographs were digitized using a Microtek ScanMaker i900 scanner at a pixel size of 5.0 Å on the specimen. To record interactions of the micelle with the transitioned pore, the tip was dipped into a solution containing the prenanodisc micelle mixture (20 μM membrane scaffold protein, MSP1D1, 1.3 mM POPC, and 25 mM sodium cholate). The newly formed LF_N−PA pore−micelle complexes were then eluted from the BLI tip as described above, and the eluted sample was deposited on glow-discharged EM grids; the resultant sample was examined directly using negative stain electron microscopy. Control experiments were performed by dipping the BLI tip containing the untransitioned prepore into an equivalent micelle mixture at near-alkaline-pH conditions (pH 8.0).

Three-Dimensional Reconstruction of Micelle-Bound PA Pores. Following the successful demonstration that PA pore−micelle complex formation could be accomplished using the small scale BLI release method, a larger scale preparation was

dx.doi.org/10.1021/bi400705n | *Biochemistry* 2013, 52, 6335−6347

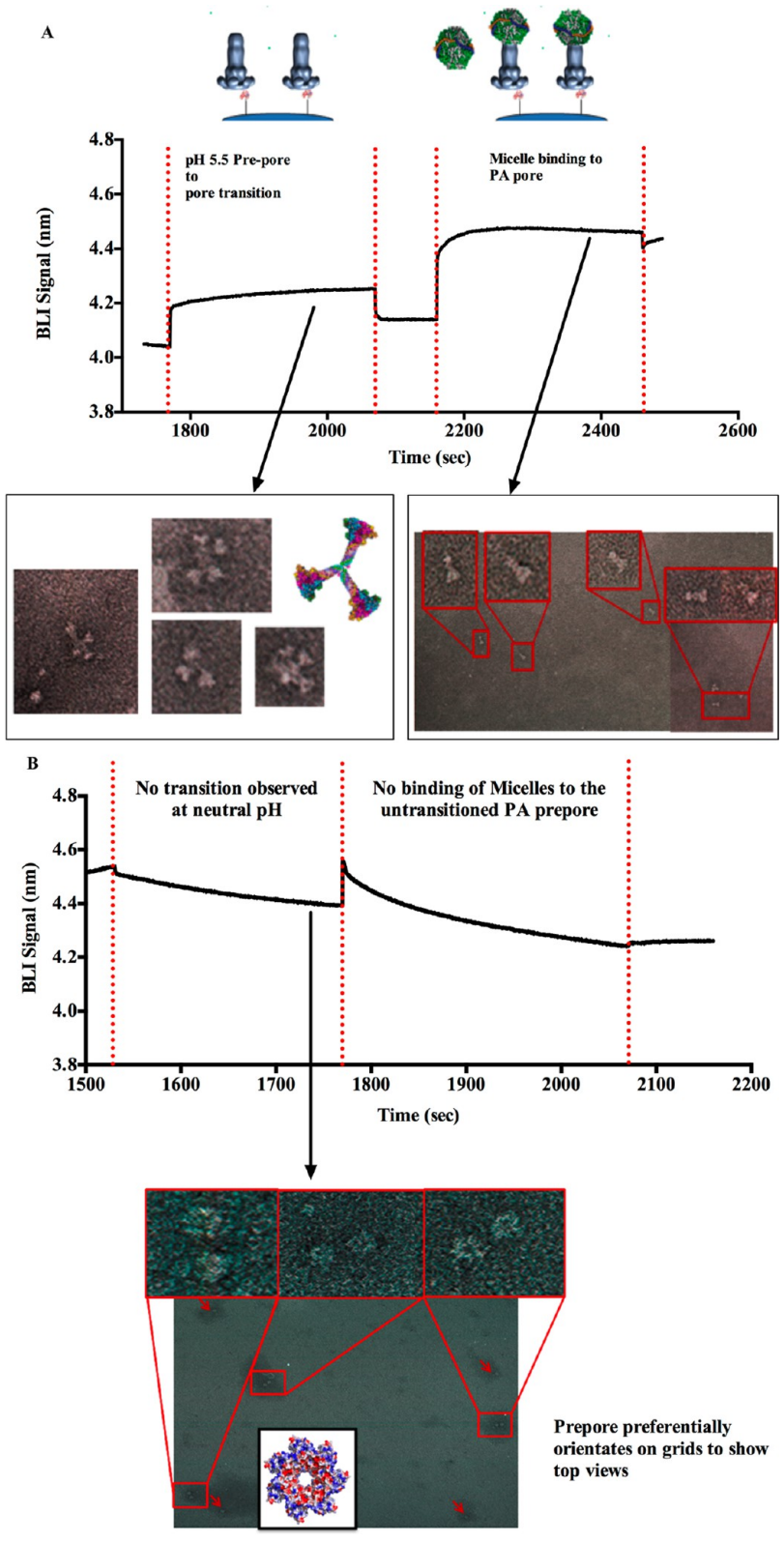

Figure 3. Electron microscopy of complexes released from BLI biosensor tips. Panel A shows that the transition occurs when the BLI tip containing the LF_N–PA prepore complex is dipped into a pH 5.0 solution. The LF_N–PA complex was removed from the biosensor tip with DTT, and the complex was deposited onto a glow-discharged copper grid. Two sets of transitioned pores released from the BLI tips were observed in the absence and presence of POPC/MSP/cholate micelles on negatively stained EM micrographs (below BLI kinetic traces in panel A). In the absence of the micelles, the pH 5.0 transitioned pores that eluted from the BLI tips show distinct PA pore aggregates that interact through the exposed hydrophobic tips (left EM micrograph and cartoon). Addition of a prenanodisc micelle to the immobilized transitioned PA pores (far right kinetic trace) shows a distinct increase in the magnitude of the BLI signal, suggesting that the micelle can interact with the PA pore. Elution and visualization of this LF_N–PA–micelle complex by EM shows a transitioned PA pore inserted into micelles as individual PA pore structures (right EM micrographs in panel A). In the control experiments (B), the prepore was attached to the BLI biosensor chip via the LF_N interaction, but the pH conditions were maintained under near-alkaline

dx.doi.org/10.1021/bi400705n | *Biochemistry* 2013, 52, 6335–6347

Figure 3. continued

conditions (pH 8.0). Under these conditions, no upward deflections of the BLI signal are observed in the absence or presence of the POPC/MSP/cholate micelles. In this panel, the EM micrographs the DTT-eluted LF_N–PA complex incubated at a constant pH of 8.0 shows individual particles that resemble typical face-up prepore heptamer complexes. No PA pore side views (aggregated or micelle-inserted) were observed in this EM micrograph (bottom EM image in panel B).

initiated to obtain a three-dimensional structure of a micelle-solubilized pore. The larger scale bead-released complexes were used to generate sufficient amounts of individual pore particles to obtain a low-resolution structure of the PA pore–micelle complex using negative stain single-particle analysis. LF_N E126C-thiol Sepharose beads were prepared as described previously;[8] 50 μL of LF_N affinity beads was transferred to a mini-spin column (Pierce Centrifuge Columns, 0.8 mL, Thermo Scientific) and washed with pH 8.0 buffer [50 mM NaCl and 50 mM Tris-HCl (pH 8.0)] and then bound to 100 μL of 0.2 μM PA prepore. Prepore to pore conversion was induced by incubating either in pH 5.5 buffer [50 mM sodium acetate and 50 mM NaCl (pH 5.5)] or at 37 °C in the presence of 1 M urea. Both methods generated a substantial number of transitioned PA pores. After the pore transition had occurred, beads were washed in a pH 8.0 Tris-HCl buffer and transferred into small microcentrifuge tubes containing 1 mL of the micelle mixture. Bead suspensions containing the micelle mixture were incubated for 30 min at 4 °C with gentle rocking agitation. Then beads were transferred to mini spin columns and washed with pH 8.0 buffer for a minimum of 20 column volumes to remove unbound micelles. E126C disulfide-attached LF_N–PA pore–micelle complexes were released from the immobilizing bead support with 50 mM DTT, and this treated and released LF_N–PA pore–micelle sample was used for EM grid preparation.[8] Samples were examined as described above; 40 micrographs were used to select particles and perform reference-free two-dimensional (2D) alignment using EMAN1.[14] Two prominent populations were observed, and three-dimensional (3D) reconstruction was performed on each of these populations using projection matching implemented in the Spider software suite.[15] To construct the initial model, the previously calculated 3D structure of PA was filtered to 100 Å resolution.[9,16] The resolution was estimated from the Fourier shell correlation curve using the FSC-0.5 cutoff criterion. Three-dimensional structures were displayed at the 100% threshold volume of the protein complex using Chimera.[17]

RESULTS

Constructing Immobilized PA Prepore Complexes and Detection of pH-Induced Transitions. To develop a system for detecting the protective antigen pore transition with label-free kinetic methods, it is crucial to bind and position the protective antigen prepore in an orientation that allows the pore transition to occur away from the biosensor surface. This specific orientation was accomplished by using the methods outlined by Akkaladevi et al.[8] that were shown to reliably generate purified PA–pore–nanodisc complexes for single-particle reconstruction and avoids aggregation. Briefly, E126C LF_N was covalently attached on both SPR and BLI biosensor surfaces via a disulfide linkage to position the lethal factor so it can easily bind to the prepore cap region, orienting the bound prepore above the biosensor surfaces. This affinity specific positioning allows the 100 Å PA pore β barrel formation to extend above the biosensor surface (Figure 1), generating an observable signal.

As predicted, the introduction of buffers mimicking gradual decreases in pH (that occur during endosomal acidification) onto the SPR or BLI biosensor surfaces containing oriented prepore arrays results in an observable increase in the magnitude of the signal in resonance units (SPR) and phase shifts (BLI) (Figure 2). For both label-free instrument platforms, this elevated and stable signal does not return to the original preacidification baseline when a pH 7.5 buffer was reintroduced into the immobilized and transitioned PA pore arrays. Control experiments using the same buffers with the lethal factor alone showed virtually no changes in signal compared to the effects observed with the PA prepore was attached.

In vivo, the prepore to pore transitions occur while the PA prepore heptamer (or octamer) is bound to cell surface receptors. Furthermore, it appears that these transitions occur when the endosome is acidified to pH 5.5–5.0.[2,18,19] In the absence of receptors, previous work indicated that the pore transition also occurs under mildly acidic pH conditions.[7,20] Both label-free systems show kinetic traces that increase in rate (and amplitude up until PA prepore binding is saturated) as the final pH of the buffer is incrementally decreased from pH 7.5 to 5.0 [Figure 2 (SPR in panel B and BLI in panel D) and Figure 1 of the Supporting Information (BLI)]. The rates of the observed pH-induced transitions for both label-free systems are listed in Table 1. Representative kinetic fits to the BLI raw data are presented in panels A and B of Figure 2 of the Supporting Information. The prepore to pore transition kinetic traces for the BLI (Figure 2D) indicate that the pH transition kinetic profiles at pH 6.75 and 6.5 are easily resolved. At a more acidic pH value of pH 5.5 or 5.0 (SPR in Figure 2B and BLI in Figure 1 of the Supporting Information), the kinetic transitions are more rapid and the initial kinetic profiles exhibit a rapid burst phase (k_1 in Table 1 from BLI and the inset of Figure 2B of the Supporting Information) that is too fast for the Biacore 3000 SPR instrumentation to resolve. The SPR sensograms showed a small, distinct, and reproducible initial overshoot of the transition signal as the pH of the flow buffer was decreased to 5.5 or 5.0 (Figure 2B). Because the PA prepore undergoes partial unfolding of the domain 2 antiparallel β loop followed by folding into the β barrel, it may be possible that these initial unfolding and refolding events are responsible for the overshoot. We chose not to pursue the origin of this overshoot in detail. The BLI signals do not show this overshoot signal as the transition pH approaches "late endosomal" pH conditions of pH 5.5 and 5.0 (Figures 1 and 6B of the Supporting Information).

Real-Time Monitoring of PA Pore–Micelle–Nanodisc Complex and Visualization by Electron Microscopy. To conclusively demonstrate that these signals correspond to PA conformational changes, one can specifically use the BLI biosensor system in conjuction with electron microscopy to verify that the PA prepore has undergone the transition to the PA pore. The immobilized transitioned pore complex can be easily removed from the BLI biosensor by reducing sulfhydryl-linked LF_N–PA pore complexes from the BLI fiber optic tip with 1 M DTT at pH 8.0 and examining the released complexes on EM micrographs.[8,9] The mildly alkaline pH of the DTT elution buffer

dx.doi.org/10.1021/bi400705n | *Biochemistry* 2013, 52, 6335–6347

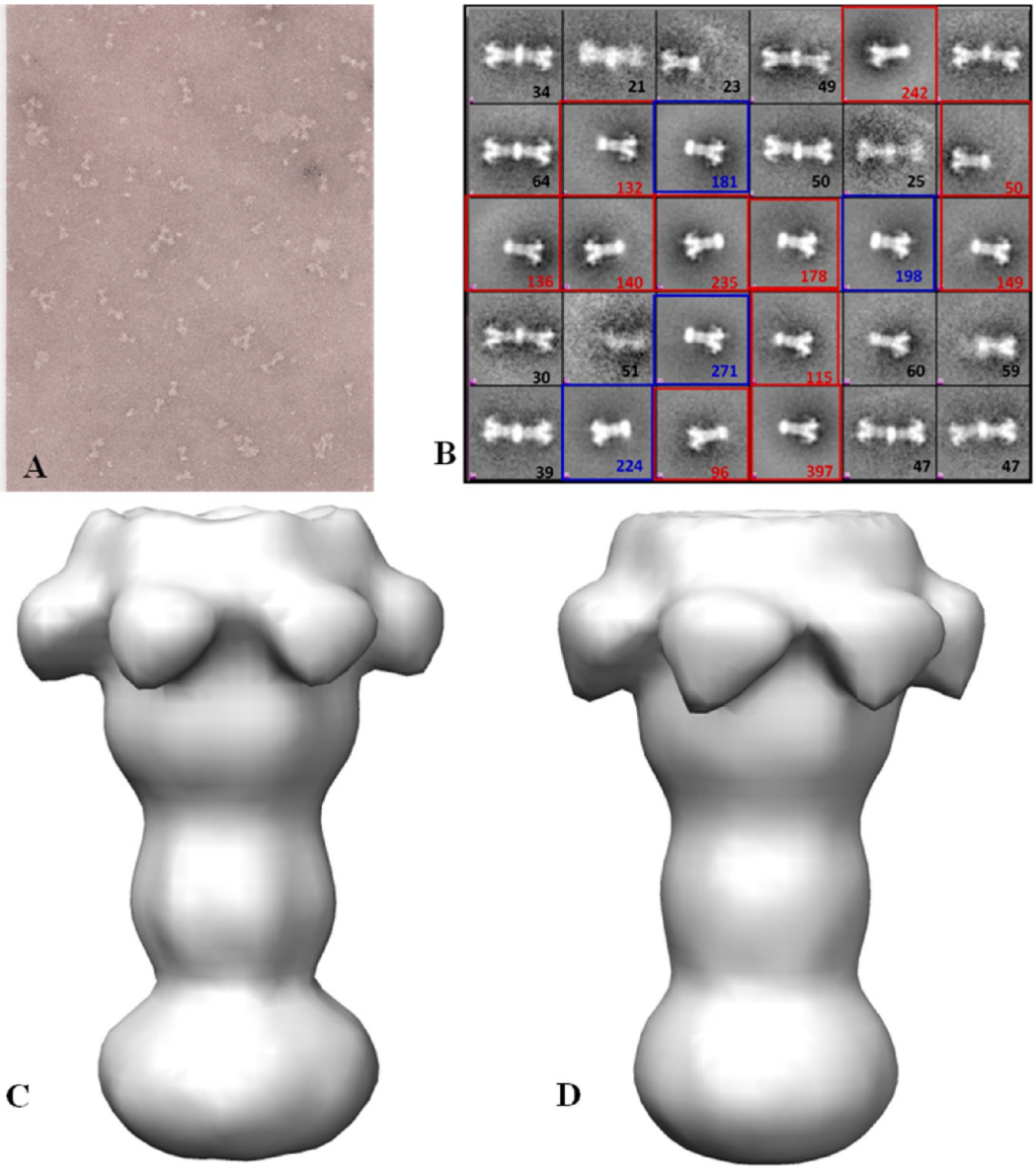

Figure 4. Scale-up of the BLI microvolume EM method to generate three-dimensional reconstructions of PA pore micelles. Panel A shows a representative negatively stained EM field of the large scale procedure to generate the MSP/cholate/POPC micelle (prenanodisc micelle) solublized pore that underwent the transition from thiol bead surfaces. (B) A total of 3369 LF_N–PA micelle particles were picked to perform reference-free 2D class averages and generate 30 separate classes. These classes contain larger ellipsoid prenanodisc micelle-solublized pores highlighted with red square boxes (reconstruction C), single-pore inserted smaller rounded prenanodiscs (reconstruction D) highlighted with blue square boxes, and a fair number of doubly inserted pore into nanodiscs. (C and D) Negative stain 3D structures of first two prominent LF_N–PA pore classes at 26 Å. The two prominent classes of prenanodisc micelles that coalse around the PA pore tip appear as expanded ellipsoid (C) or smaller round (D) densities.

was used to ensure that no additional PA prepore could undergo the transition to the pore form prior to EM preparation (see Figure 3B). The amount of complex that can be released into solution from a single 600 μm diameter BLI tip can be quite substantial if the release solution volume is small. It is estimated that in a final volume of 2 μL the approximate final concentration of PA pore complexes (oligomers) can be between 1 and 3 pM. The resulting electron micrograph fields verified that adequate quantities of the free LF_N–PA pore complex (144 Å × 210 Å) can be released from the tips to assess the pore transition efficiency using electron microscopy. Previous experiments by Katayama et al.[16] and Akkaladevi[8] demonstrated that released PA pores or PA–nanodisc pores (nearly the same dimensions) can be routinely and easily observed using standard negatively stained electron microscopy. In control experiments, the LF_N–PA prepore complex was maintained under near-neutral solution conditions (pH >7.5), and this untransitioned prepore complex was also released onto an EM microscopy grid using the same DTT elution buffer (pH 8.0) (Figure 3B).

As shown in panels A and B of Figure 3, a large number of tip-released pure individual PA molecules could be observed on the EM grids. The electron micrograph images of the released LF_N–PA pore complex (generated with pH 5.5 buffer for these experiments) shows the distinct side view orientation of the cap region (Figure 3A) that is observed only when the anthrax toxin pore is present in its transitioned form on the glow-discharged EM grids.[8,16,20] Furthermore, in the absence of detergents or other solubilizing agents (i.e., micelles), the transitioned pores

dx.doi.org/10.1021/bi400705n | *Biochemistry* 2013, 52, 6335–6347

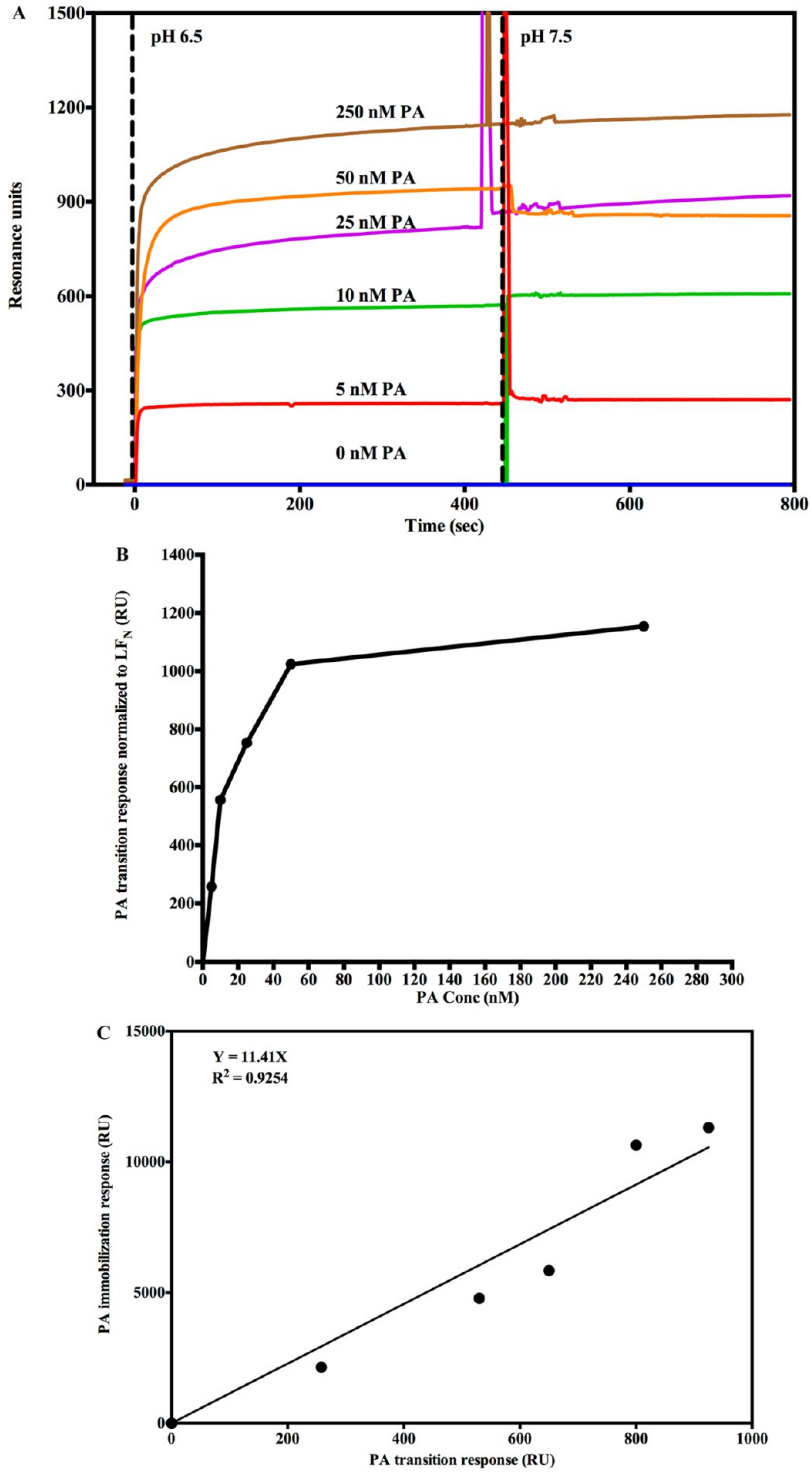

Figure 5. pH jump (pH 7.5 to 6.5) SPR signal that correlates with the amount of prepore that is initially bound to the chip surface. The transition amplitudes were normalized with respect to the amount of LF_N being immobilized on the surface. (A) The kinetics of the transition are approximately equivalent and independent of the amount of prepore loaded onto the SPR chip. (B) The transition amplitude levels off at high prepore loading concentrations, presumably because of the saturation of PA prepore binding. (C) The prepore loading amplitudes are linearly correlated with the pore transition amplitude. The correlation coefficient is 0.92 for the zero force fit.

naturally interact through their exposed hydrophobic tip regions[20] to form small rosette aggregates composed of complexes anywhere from two to four separate pores. The preferential side view orientation shows the characteristic Y shape making up the cap region connected to the extended β barrel of the transitioned pore. In contrast, at pH 7.5−8.0 (near-alkaline conditions), the LF_N−PA prepore complex remains in its prepore form (see EM micrographs in Figure 3B). The prepore form of PA preferentially lies face up on the EM grid showing a distinct central cavity and does not form large aggregates within the EM fields. These EM images verified that the transitions observed on the BLI biosensor tips were prepore to pore

dx.doi.org/10.1021/bi400705n | *Biochemistry* 2013, 52, 6335−6347

transitions and provide strong evidence that the kinetic signals generated by SPR or BLI correspond to the transition of the PA prepore to the pore.

In a separate experiment, the complete kinetic traces of both the PA pore transition and the insertion of PA pore tip into POPC/MSP/cholate micelles on the BLI biosensor could be easily observed in sequence (Figure 3A). An upward BLI signal deflection suggesting micelle binding was observed only when PA undergoes the transition to its membrane insertable pore form (Figure 3A). In contrast, similar experiments with the PA prepore showed no such upward deflection (Figure 3B). The micelle-solubilized PA pore complexes released from the BLI tip do not show any pore−pore tip aggregation, and the distinct LF_N−PA pore micelle complexes were easily resolved on the EM micrographs as individual particles (right-hand side, Figure 3A). These results indicate that one can solubilize the PA pores by adding micelles, which in turn can define solution conditions that can generate enough PA pore−micelle complexes for single-particle analysis.

EM Reconstruction of PA Pore−Micelle Complexes. The BLI results coupled with EM analysis indicate that the LF_N−PA pore−micelle complex can be assembled on and released from a solid support surface. This should allow one to generate significant quantities of soluble LF_N−PA pore−micelle complexes for single-particle analysis. To verify that PA pore−micelle complexes can be produced in larger quantities, a scaled-up purification of the LF_N−PA pore−micelle complex based on the BLI release method was implemented by using LF_N-thiol Sepharose beads as the reversible covalent attachment platform.[8] The PA prepore bound noncovalently to the oriented LF_N, and the transition was induced by acidification or incubation with 1 M urea at 37 °C in the presence of MSP/POPC/cholate micelle mixtures. The disulfide-linked complexes were released from the bead surface using DTT, and the integrity of these soluble complexes was assessed using negative stain electron microscopy. A representative EM field is shown in Figure 4A. The imaged fields were digitized (total of 40 EM fields), and 3369 particles were manually selected by using EMAN1.[14] Reference-free 2D alignment was applied to the selected image particles, and *k*-means classification was performed using EMAN1, allowing separation of the image populations into roughly 30 classes (Figure 4B). Three prominent populations were observed from 30 classes: one class of PA pore was inserted into ellipsoid prenanodisc micelles, another class of PA pores was inserted into circular prenanodisc micelles, and a third prominent class of particles contained two PA molecules inserted into what appears to be more of a nanodisc-shaped disk. These prominent particle populations were separated into three groups, 874 LF_N−PA−ellipsoid prenanodisc micelles, 1870 LF_N−PA−circular prenanodisc micelles, and 432 particles with two PA molecules inserted into a single nanodisc. The first two image data sets were used for a preliminary 3D analysis, yielding structures with a nominal resolution of 26 Å (Figure 4C,D). 3D structures are similar to previously determined PA pore complexes inserted into lipid nanodiscs[8,16] and PA pores bound to the chaperonin GroEL.[20]

Correlation of the PA−LF_N Complex Concentration with Transition Signals. If an authentic prepore to pore transition occurs on the biosensor surfaces, then one would also predict that the starting PA concentration SPR signal amplitude would correlate in a linear fashion with the signal of the corresponding PA transition. To test for the predicted quantitative relationship, increasing concentrations of PA (0−250 nM) were allowed to interact with a fixed amount of covalently immobilized LF_N (starting concentration of 100 nM). These were then acidified using pH 6.5 buffer, and the increase in the magnitude of the signal due to the PA transition was recorded (Figure 5A). The PA binding signal on the SPR sensorgram was then compared with the PA transition signal after acidification at pH 6.5. The PA binding amplitudes were normalized to the LFN binding signal to account for slight differences in PA immobilization. As the PA prepore concentration that flows over the immobilized LF_N increases, the amount of PA prepore that can bind to the chip approaches a saturable limit and the PA pore transition signal levels off (Figure 5B). The PA binding amplitude signals and PA transition amplitude signals are linearly correlated (Figure 5C). Raw (not normalized to initial LF_N binding) PA binding amplitudes were also linearly correlated with the PA pH-induced transition signals (data not shown).

Effects of Soluble ANTXR2 and CMG2 Receptor Binding on PA Prepore to Pore Transition Kinetics. The data presented thus far indicate that PA prepore to pore transitions can even be observed at near-neutral pH values of 6.5−6.8, albeit with slower transition kinetics (Figure 2, Figure 1 of the Supporting Information, and Table 1). The data also agree with previous instances in which transitions were readily observed under similar conditions within lipid bilayers and in solution.[6,7] The lower amplitudes and slower transitions under less acidic conditions (pH ≥6.0) may indicate that not all of the bound PA prepore undergoes the transition to the pore within the experimental time frame. *In vivo*, PA pore transitioning and accompanying LF or EF translocation occurs within the endosome once the pH values reach 5.0−5.5[19] during late stage endosome maturation. The *in vivo* pH threshold of the PA prepore to pore transition depends on the type of receptor that binds the PA prepore.[21,22] Tighter binding receptors such as ANTRX2 (CMG2) decrease the pH threshold of the PA pore transition to ∼5.2, while the PA pore transition with the weaker binding receptor, ANTXR1 (TEM8), occurs at a higher pH of 6.2. This differential pH dependency for the receptor-bound PA pore transitions correlates with the strength of the interaction of the receptor with the PA prepore. Stronger receptor−PA prepore interactions constrain the unfolding−refolding movements of the D2L2 loop at the domain 4−domain 2 interface.[23−25] This loop is the structure that undergoes the largest-magnitude unfolding and refolding as the prepore undergoes the transition to the β barrel stem.[7] Therefore, it was predicted that receptor binding should stabilize domain 2 against pH-dependent unfolding, leading to an inhibition of the SPR- and BLI-dependent prepore to pore transition signals at near-neutral pH values of >6.5.

The positioning of the immobilized prepore on the biosensor surface should allow one to effectively observe the soluble CMG2 domains binding to the PA prepore. For the SPR and BLI experiments, a saturating amount of PA prepore (250 nM) was preloaded onto the oriented LF_N on the biosensor surface, which in turn orientes the receptor binding interface (encompassing PA external surfaces comprised of domains 4 and 2) for optimal receptor binding. In these experiments, ∼500 nM soluble CMG2 was passed over the SPR sensor surface (A) or dipped onto the immobilized LF_N−PA complex BLI surface to eventually form the LF_N−PA−CMG2 complex (complete SPR sensorgram shown in Figure 3 of the Supporting Information). With both label-free systems, the receptor−prepore complex forms readily and does not show any substantial dissociation following a buffer chase (SPR in Figure 3 of the Supporting Information and BLI in

dx.doi.org/10.1021/bi400705n | *Biochemistry* 2013, 52, 6335−6347

Figure 6C). The lack of any appreciable decrease in the dissociation kinetics agrees with the observation that the binding affinity of CMG2 or ANTXR2 for the PA prepore is tight ($K_d \simeq$ 170 pM).[26]

The LF_N−PA−CMG2 complexes that are exposed to pH >6.5 solutions show no apparent kinetic transitions as assessed by either SPR or BLI label-free systems (Figure 6A,B). In the SPR sensorgram, a slight upward signal (green trace) was observed only when the pH was decreased to 5.5 (Figure 6A). When the pH of the flow or dip buffers was decreased 5.0, the sensorgrams of the SPR and BLI show a sharp rise in the magnitude of the signal followed by a large gradual decline in the magnitude of the signal. This initial sharp upward signal deflection most likely corresponds to the pore transition, and the subsequent decline appears to correlate with CMG2 receptor dissociation.[22] Consistent with the notion that the initial signal corresponds to a pore transition, the amplitude of this initial rise in the magnitudes of both SPR and BLI signals corresponds to the expected increase observed for pore formation in the absence of the receptor (Figures 2A and 6A,B). The SPR rise is slightly higher than expected, and this may be due to the contribution of a degree of CMG2 unfolding during the pH jump. The complete sensorgrams show that following the rapid initial rise in the magnitude of the signal (transition), the experimental trace returns to the original baseline signal level recorded prior to receptor binding. In the absence of the bound CMG2 receptor, PA prepore− or pore−LF_N complexes alone do not show any substantial decline in the magnitudes of signals following acidification and a return to pH 7.5 (Figure 2). These data suggest that the declines in the magnitude of the signal following acidification of the complete complex (LF_N−PA−CMG2) are most likely due to soluble CMG2 receptor dissociation. This suggestion was also supported by the observation that the CMG2 binding interaction with the pH-transitioned PA pore is significantly weakened (Figure 6C, blue trace).

DISCUSSION

The transitions observed with these immobilized anthrax toxin complexes recapitulate, in part, the pH-induced changes that occur in the endosome as the PA prepore unfolds and refolds into its pore conformation. At pH 5.0, the transition shows a substantial rapid burst phase and the magnitude of this kinetic change is essentially 80% complete within the first 5 s using both the SPR and BLI biosensor platforms. A similar kinetic transition, including a distinct rapid burst phase (k_1 in Table 1 and shown in Figure 2 of the Supporting Information), was previously observed by Vernier et al.; they measured the kinetic changes in circular dichroism ellipticity at 218 nm as the PA prepore undergoes the transition to its pore form in the presence of the detergent *N*-tetradecylphosphocholine (FOS14) at pH 5.5.[27] The k_2 and k_3 kinetic constants obtained from the kinetic fits to the BLI data (Table 1) agree quite well with the k_1 and k_2 constants measured by CD.[27] In the latter kinetic analysis,[27] the initial kinetic rate constant of the burst phase (k_1 in Table 1 and shown in Figure 2 of the Supporting Information) was not measured because the initial kinetic data points were not resolved. Indirect kinetic measurements of the PA pore transition into K^+-loaded Ni^{2+}-doped liposomes starting from preloaded PA prepore−His-tagged CMG2 receptor complexes show implied transition rates that are also consistent with our label-free kinetic measurements.[29] The rapid release of K^+ due to a combination of PA pore formation and pore insertion at pH 5.0 has a half-life of several seconds; the kinetic traces appear to be

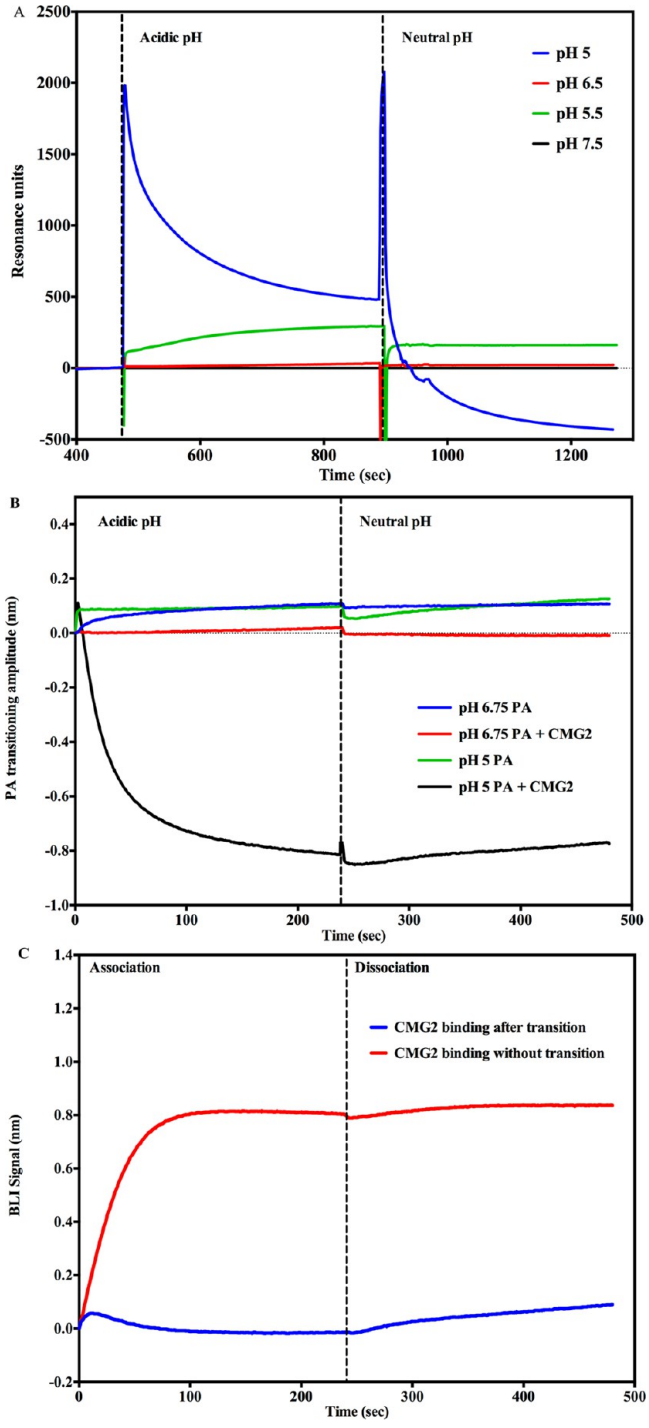

Figure 6. pH-induced transition in the presence of the soluble CMG2 receptor (0.5 μM). (A) Receptor binding inhibits acid-induced transitions above pH 5.5 as assessed by SPR. No significant pH-induced transitions were observed (green and black traces) until the flow buffer pH was decreased to 5.5 (green trace). At pH 5.0 (blue trace), there was an initial rapid rise followed by a decline in amplitude consistent with the transition of the PA prepore to the pore followed by receptor dissociation. The spike observed at ~900 s is due to a shift in pH from acidic to neutral. (B) BLI biosensor traces indicate that acid-induced transitions at pH 6.75 (blue trace) are inhibited (red trace) when the CMG2 receptor is initially bound to the prepore. At pH 5.0, the prepore rapidly shows a rapid acid-induced transition (green trace). In the presence of the CMG2 receptor (0.5 μM), the magnitude of the BLI signal initially increases to the pH 5.0 transition amplitude [without CMG2 present (green trace)] and sharply declines to a level that nearly

dx.doi.org/10.1021/bi400705n | *Biochemistry* 2013, 52, 6335−6347

Figure 6. continued

matches the initial baseline of the prepore prior to receptor loading (just above −0.8 nm) (black trace). (C) The BLI sensorgram shows that binding of soluble CMG2 (0.5 μM) to the immobilized prepore (pH 7.5) results in a large upward deflection in the signal (red trace) (+0.8 nm). Very little CMG2 dissociates from the complex when the tip is dipped into a solution without CMG2 (dissociation phase). In contrast, if the prepore undergoes a transition in pH to the pore on the BLI biosensor (pH 5.0) prior to the tip being returned (dipped) to the 0.5 μM CMG2 solution at pH 7.5, very little PA pore−CMG2 receptor binding signal is observed during the association phase (blue trace).

multiphasic with an initial burst phase, and the kinetics of K^+ release are essentially complete within ∼60 s in near agreement with the BLI and SPR kinetic measurements. The kinetic measurements from the BLI-measured transition at pH 6.75−5.0 all show a minimum of three phases (Figure 2 of the Supporting Information and listed in Table 1). The fits to the kinetic data show a slight overshoot in the residuals, particularly at the lower endosomal-like pH values within the first kinetic phase, indicating that the transition is probably more complex as the pH approaches endosomal solution conditions (insets of Figure 2A,B of the Supporting Information). This is a reasonable assumption considering the large scale unfolding, refolding, and reassembly processes that have to occur during the prepore to pore transition.

The presence of the bound soluble CMG2 receptor to the PA prepore slows pore transitions at pH 5.5 (Figure 6A and Figure 3 of the Supporting Information) and completely inhibits these transitions at pH ≥6.0. When the PA prepore to pore transition is induced at pH 5.0 in a more complete endosomal complex including the soluble receptor (LF_N−prepore−CMG2), the prepore transition to the pore shows a rapid rise followed by a large decline that is attributed to the pore transition followed by receptor dissociation (Figure 6A,B). Dissociation of the receptor elicits a large signal diminishing in magnitude that inversely agrees with the correlative increase in the association signal of receptor binding to the prepore complex. The positive receptor binding deflection signal is always much larger than the positive signal generated by the pore transition. Furthermore, the rapid dissociation of the receptor from the transitioned pore leads one to predict that the binding between the receptor and the pore should be weakened as the pH approaches 5.0. In fact, when one attempts to measure the binding of the soluble CMG2 receptor to a transitioned PA pore attached to the BLI tip using the same CMG2 concentrations used to construct the LF_N−PA prepore−CMG2 complex, virtually no binding signal is observed under neutral extracellular pH conditions [pH 7.0−7.5 (Figure 6C)]. This direct observation agrees with NMR-based observations that the PA−receptor interactions become weaker as the prepore undergoes the transition to the pore.[28] Because our complex is anchored to an immobilized surface in the opposite orientation that occurs *in vivo* (i.e., prepore bound to membrane-anchored CMG2), it is premature to firmly conclude that the receptor dissociates completely after pore formation *in vivo*. Certainly, a weakened receptor interaction (loss of domain 2 interaction and decrease in the extent of domain 4 interactions) allows the pore transition to occur, and a weakened receptor−PA pore affinity is reflected in an increased level of dissociation of the receptor from the completely transitioned pore.[22] Our results agree with this sequence of interactions and indicate that binding of the receptor to the transitioned pore is considerably weaker than binding of the receptor to the prepore because no receptor−pore interactions could be observed and the receptor rapidly dissociates from PA once the prepore undergoes the transition to the pore. After the transition to the PA pore in the presence of the soluble receptor, both the SPR and BLI signal amplitudes return to the original baseline that was recorded before the soluble receptor bound to the PA prepore. This again supports the contention that there is a substantial or nearly complete dissociation of the receptor from the LF_N−PA pore complex at pH 5.0 in either the SPR flow or BLI-dipped solutions because each of these dissociation solutions could no longer contain the soluble receptor.

Another highlight of the work presented herein is the demonstration that one can easily use the smaller detachable BLI biosensors to capture and release the assembled complexes onto EM grids using reversible disulfide linkages, thus allowing one to determine directly the conformation of the large PA pore molecular complexes using electron microscopy. The ability to observe the kinetic transitions and validate the nature of the macromolecular conformational changes that occur on a label-free platform allows one to both identify and fine-tune complex formation or transitions. Our ability to couple label-free methods with EM methods helped us (1) validate that the PA pore transition had occurred, (2) demonstrate that a soluble micelle will bind to the exposed pore hydrophobic tip, and (3) demonstrate that, once formed, this immobilized PA pore micelle complex is released as soluble individual particles. These successful microvolume test experiments serve as proof-of-principle examples that then allow us to scale up the procedure to assemble larger sample preparations for image analysis and three-dimensional reconstructions of PA−pore prenanodisc micelle complexes. The ease of directly releasing and examining macromolecular complexes that assemble or undergo the transition on BLI tips should be readily applicable in visualizing the molecular structure of other high-molecular mass complex systems. In these instances, one can potentially visualize other large size macromolecular structures that assemble on BLI tips that also would correlate with BLI kinetic results. It is entirely possible that this combination of BLI and electron microscopy can be further exploited to follow the folding and assembly of a wide range of soluble protein complexes and membrane protein micelle complexes.

There has been some progress in the development of high-throughput screens to identify potential inhibitors of the anthrax toxin internalization and PA pore transition. Using a cell-based system, Leppla and colleagues[30] were able to identify a number of potential inhibitors of anthrax toxin-induced cell death. In these indirect screens, numerous lead compounds were found to inhibit the prepore to pore transition and subsequent lethal factor translocation. Interestingly, these anti-anthrax small molecule candidates appear to inhibit the endosomal acidification process because these same lead compounds also inhibited other toxin systems that also require endosomal acidification. Another target for the development of novel anti-anthrax compounds involves inhibiting the initial interactions between the anthrax receptors (TEM8 or CMG2) and PA prepore monomers or oligomers.[31]

The label-free anthrax toxin platforms described herein can potentially be used as test systems to identify direct molecular inhibitors of endosomal transitions in a high-throughput screening platform. Both the direct label-free detection platform presented here and the indirect cellular system mentioned above allow one to identify potential inhibitors of pathogenic pathways

while avoiding the cumbersome implementation of stringent biosafety constraints. As one compares this method with other potential high-throughput methods, the label-free methods can potentially identify direct inhibitors of the molecular transition compared with the other indirect cell-based methods. It is important to note that the cell-based methods are absolutely essential for validating the *in vivo* relevance and efficacy of potential anti-anthrax lead compounds that can be identified with the BLI or SPR pore transition screens. The K^+ release liposome assay[29] can also serve as a high-throughput platform system but is still one step removed from a direct measurement. The CD transition measurement in detergents[27] also examines the direct pore transitions and is therefore another direct method, but this method may be difficult to scale up to a high-throughput system because one has to implement rapid mixing procedures at higher concentrations.

The SPR or BLI label-free platforms can be used to rapidly access the dynamics of many aspects of the anthrax complex formation and molecular transitions that occur as the pH approaches endosomal solution conditions. In addition to monitoring the pH-dependent pore transitions directly, our ability to easily follow and validate the formation of these complexes on the same biosensor surfaces can be used to identify potential small molecule inhibitors of the assembly of pretransition endosomal complexes. Both the pore transitions and each of the individual binding steps (i.e., PA prepore−LF_N binding and receptor−PA prepore interactions) are all valid target platforms that can be used to screen, identify, or validate potential new classes of antimicrobial compounds that function under either neutral- or endosomal-pH conditions.

Because the CMG2−prepore structures are known, one may be able to use these initial complexes to identify small molecule candidates identified by virtual screens that bind to potential druggable sites in hopes that they may strengthen the interactions of the receptor with the prepore. Using BLI or SPR label-free approaches, one could then directly test if synthesized protein stabilizer candidates inhibit the PA pore transitions in endosomal-like solution environments. A similar *in silico* approach was implemented by Wein et al., where they used initially used virtual screening methodologies to identify potential inhibitors of PA prepore oligomerization.[32] They then tested a number of positive candidates directly using cell-based systems and found that in addition to oligomer inhibition, some of these compounds also inhibited the furin-based proteolytic processing of the PA protective antigen.[32]

In a broader sense, it is quite conceivable that our ability to monitor direct endosomal-like transitions of anthrax toxin complexes with label-free methods can also serve as a general methodological approach to constructing and directly monitoring the endosomal transitions of other complex bacterial toxin- or viral protein-based assembly systems. As summarized above, the ability to specifically assemble multiple component toxin protein systems on label-free platforms has the advantage of providing multiple screening targets for identifying inhibitors of numerous toxin specific protein−protein interactions. More uniquely, the ability to assemble pre-endosomal toxin complexes using label-free approaches should allow one to directly target and inhibit toxin-dependent molecular transitions that occur as the endosome becomes acidic.

■ ASSOCIATED CONTENT

Supporting Information

BLI sensorgrams of transitions measured for the channel BLI unit (Figure 1), kinetic fits to the octet and BLItz BLI data (Figure 2), and uncorrected complete SPR LF_N−PA prepore−CMG2 construction and pore transition sensorgrams (Figure 3). This material is available free of charge via the Internet at http://pubs.acs.org.

■ AUTHOR INFORMATION

Corresponding Author

*Department of Biochemistry and Molecular Biology, University of Kansas Medical Center, Kansas City, KS 66160. E-mail: mfisher1@kumc.edu. Telephone: (913) 588-6940. Fax: (913) 588-9896.

Funding

This work was supported by National Institutes of Health (NIH) Grant R01AI090085 (M.T.F.), NIH Grant SR37AI022021 (R.J.C.), National Center for Research Resources Grant 5P20RR017708-10, and National Institute of General Medical Sciences Grant 8P20 GM103420-10 (N.Z. and P.G.).

Notes

The authors declare no competing financial interest.

■ ABBREVIATIONS

PA, protective antigen; LF, lethal factor; LF_N, N-terminal fragment of the lethal factor; EF, edema factor; SPR, surface plasmon resonance; BLI, biolayer interferometry; CMG2, capillary morphogenesis protein 2; TEM8, tumor endothelium marker 8; ANTXR1, anthrax toxin receptor 1; ANTXR2, anthrax toxin receptor 2; POPC, 1-palmitoyl-2-oleoyl-*sn*-glycero-3-phosphocholine; PDEA, 2-(2-pyridinyldithio)ethaneamine hydrochloride; EDC, 1-ethyl-3-[3-(dimethylamino)propyl]-carbodiimide hydrochloride; NHS, *N*-hydroxysuccinimide ester; PDB, Protein Data Bank.

■ REFERENCES

(1) Kintzer, A. F., Sterling, H. J., Tang, I. I., Williams, E. R., and Krantz, B. A. (2010) Anthrax toxin receptor drives protective antigen oligomerization and stabilizes the heptameric and octameric oligomer by a similar mechanism. *PLoS One 5*, e13888.

(2) Wesche, J., Elliott, J. L., Falnes, P. O., Olsnes, S., and Collier, R. J. (1998) Characterization of membrane translocation by anthrax protective antigen. *Biochemistry 37*, 15737−15746.

(3) Zako, T., Harada, K., Mannen, T., Yamaguchi, S., Kitayama, A., Ueda, H., and Nagamune, T. (2001) Monitoring of the refolding process for immobilized firefly luciferase with a biosensor based on surface plasmon resonance. *J. Biochem. 129*, 1−4.

(4) Chen, L. Y. (2009) Monitoring conformational changes of immobilized RNase A and lysozyme in reductive unfolding by surface plasmon resonance. *Anal. Chim. Acta 631*, 96−101.

(5) Paynter, S., and Russell, D. A. (2002) Surface plasmon resonance measurement of pH-induced responses of immobilized biomolecules: Conformational change or electrostatic interaction effects? *Anal. Biochem. 309*, 85−95.

(6) Blaustein, R. O., Koehler, T. M., Collier, R. J., and Finkelstein, A. (1989) Anthrax toxin: Channel-forming activity of protective antigen in planar phospholipid bilayers. *Proc. Natl. Acad. Sci. U.S.A. 86*, 2209−2213.

(7) Miller, C. J., Elliott, J. L., and Collier, R. J. (1999) Anthrax protective antigen: Prepore-to-pore conversion. *Biochemistry 38*, 10432−10441.

(8) Akkaladevi, N., Hinton-Chollet, L., Katayama, H., Mitchell, J., Szerszen, L., Mukherjee, S., Gogol, E. P., Pentelute, B. L., Collier, R. J.,

and Fisher, M. T. (2013) Assembly of anthrax toxin pore: Lethal-factor complexes into lipid nanodiscs. *Protein Sci. 22*, 492−501.
(9) Gogol, E. P., Akkaladevi, N., Szerszen, L., Mukherjee, S., Chollet-Hinton, L., Katayama, H., Pentelute, B. L., Collier, R. J., and Fisher, M. T. (2013) Three dimensional structure of the anthrax toxin translocon-lethal factor complex by cryo-electron microscopy. *Protein Sci. 22*, 586−594.
(10) Feld, G. K., Thoren, K. L., Kintzer, A. F., Sterling, H. J., Tang, I. I., Greenberg, S. G., Williams, E. R., and Krantz, B. A. (2010) Structural basis for the unfolding of anthrax lethal factor by protective antigen oligomers. *Nat. Struct. Mol. Biol. 17*, 1383−1390.
(11) Bayburt, T. H., and Sligar, S. G. (2010) Membrane protein assembly into Nanodiscs. *FEBS Lett. 584*, 1721−1727.
(12) Pimental, R. A., Christensen, K. A., Krantz, B. A., and Collier, R. J. (2004) Anthrax toxin complexes: Heptameric protective antigen can bind lethal factor and edema factor simultaneously. *Biochem. Biophys. Res. Commun. 322*, 258−262.
(13) Mogridge, J., Cunningham, K., and Collier, R. J. (2002) Stoichiometry of anthrax toxin complexes. *Biochemistry 41*, 1079−1082.
(14) Ludtke, S. J., Baldwin, P. R., and Chiu, W. (1999) EMAN: Semiautomated software for high-resolution single-particle reconstructions. *J. Struct. Biol. 128*, 82−97.
(15) Frank, J., Radermacher, M., Penczek, P., Zhu, J., Li, Y., Ladjadj, M., and Leith, A. (1996) SPIDER and WEB: Processing and visualization of images in 3D electron microscopy and related fields. *J. Struct. Biol. 116*, 190−199.
(16) Katayama, H., Wang, J., Tama, F., Chollet, L., Gogol, E. P., Collier, R. J., and Fisher, M. T. (2010) Three-dimensional structure of the anthrax toxin pore inserted into lipid nanodiscs and lipid vesicles. *Proc. Natl. Acad. Sci. U.S.A. 107*, 3453−3457.
(17) Pettersen, E. F., Goddard, T. D., Huang, C. C., Couch, G. S., Greenblatt, D. M., Meng, E. C., and Ferrin, T. E. (2004) UCSF Chimera: A visualization system for exploratory research and analysis. *J. Comput. Chem. 25*, 1605−1612.
(18) Milne, J. C., and Collier, R. J. (1993) pH-dependent permeabilization of the plasma membrane of mammalian cells by anthrax protective antigen. *Mol. Microbiol. 10*, 647−653.
(19) Milne, J. C., Furlong, D., Hanna, P. C., Wall, J. S., and Collier, R. J. (1994) Anthrax protective antigen forms oligomers during intoxication of mammalian cells. *J. Biol. Chem. 269*, 20607−20612.
(20) Katayama, H., Janowiak, B. E., Brzozowski, M., Juryck, J., Falke, S., Gogol, E. P., Collier, R. J., and Fisher, M. T. (2008) GroEL as a molecular scaffold for structural analysis of the anthrax toxin pore. *Nat. Struct. Mol. Biol. 15*, 754−760.
(21) Wolfe, J. T., Krantz, B. A., Rainey, G. J., Young, J. A., and Collier, R. J. (2005) Whole-cell voltage clamp measurements of anthrax toxin pore current. *J. Biol. Chem. 280*, 39417−39422.
(22) Rainey, G. J., Wigelsworth, D. J., Ryan, P. L., Scobie, H. M., Collier, R. J., and Young, J. A. (2005) Receptor-specific requirements for anthrax toxin delivery into cells. *Proc. Natl. Acad. Sci. U.S.A. 102*, 13278−13283.
(23) Lacy, D. B., Wigelsworth, D. J., Melnyk, R. A., Harrison, S. C., and Collier, R. J. (2004) Structure of heptameric protective antigen bound to an anthrax toxin receptor: A role for receptor in pH-dependent pore formation. *Proc. Natl. Acad. Sci. U.S.A. 101*, 13147−13151.
(24) Santelli, E., Bankston, L. A., Leppla, S. H., and Liddington, R. C. (2004) Crystal structure of a complex between anthrax toxin and its host cell receptor. *Nature 430*, 905−908.
(25) Scobie, H. M., Marlett, J. M., Rainey, G. J., Lacy, D. B., Collier, R. J., and Young, J. A. (2007) Anthrax toxin receptor 2 determinants that dictate the pH threshold of toxin pore formation. *PLoS One 2*, e329.
(26) Wigelsworth, D. J., Krantz, B. A., Christensen, K. A., Lacy, D. B., Juris, S. J., and Collier, R. J. (2004) Binding stoichiometry and kinetics of the interaction of a human anthrax toxin receptor, CMG2, with protective antigen. *J. Biol. Chem. 279*, 23349−23356.
(27) Vernier, G., Wang, J., Jennings, L. D., Sun, J., Fischer, A., Song, L., and Collier, R. J. (2009) Solubilization and characterization of the anthrax toxin pore in detergent micelles. *Protein Sci. 18*, 1882−1895.
(28) Pilpa, R. M., Bayrhuber, M., Marlett, J. M., Riek, R., and Young, J. A. (2011) A receptor-based switch that regulates anthrax toxin pore formation. *PLoS Pathog. 7*, e1002354.
(29) Sun, J., Vernier, G., Wigelsworth, D. J., and Collier, R. J. (2007) Insertion of Anthrax Protective Antigen into Liposomal Membranes: Effects of a Receptor. *J. Biol. Chem. 282*, 1059−1065.
(30) Zhu, P. J., Hobson, J. P., Southall, N., Qiu, C., Thomas, C. J., Lu, J., Inglese, J., Zheng, W., Leppla, S. H., Bugge, T. H., Austin, C. P., and Liu, S. (2009) Quantitative high-throughput screening identifies inhibitors of anthrax-induced cell death. *Bioorg. Med. Chem. 17*, 5139−5145.
(31) Cryan, L. M., Habeshian, K. A., Caldwell, T. P., Morris, M. T., Ackroyd, P. C., Christensen, K. A., and Rogers, M. S. (2013) Identification of Small Molecules That Inhibit the Interaction of TEM8 with Anthrax Protective Antigen Using a FRET Assay. *J. Biomol. Screening 18*, 714−725.
(32) Wein, A. N., Williams, B. N., Liu, S., Ermolinsky, B., Provenzano, D., Abagyan, R., Orry, A., Leppla, S. H., and Peredelchuk, M. (2012) Small molecule inhibitors of *Bacillus anthracis* protective antigen proteolytic activation and oligomerization. *J. Med. Chem. 55*, 7998−8006.
(33) Pannifer, A. D., Wong, T. Y., Schwarzenbacher, R., Renatus, M., Petosa, C., Bienkowska, J., Lacy, D. B., Collier, R. J., Park, S., Leppla, S. H., Hanna, P., and Liddington, R. C. (2001) Crystal structure of the anthrax lethal factor. *Nature 414*, 229−233.